Fluctuations of Energy-Relaxation Times in Superconducting Qubits

P. V. Klimov *et al.*

Phys. Rev. Lett. **121**, 090502 — Published 31 August 2018

DOI: 10.1103/PhysRevLett.121.090502

Fluctuations of energy-relaxation times in superconducting qubits

P. V. Klimov[1], J. Kelly[1], Z. Chen[1], M. Neeley[1], A. Megrant[1], B. Burkett[1], R. Barends[1], K. Arya[1], B. Chiaro[3], Yu Chen[1], A. Dunsworth[3], A. Fowler[1], B. Foxen[3], C. Gidney[1], M. Giustina[1], R. Graff[1], T. Huang[1], E. Jeffrey[1], E. Lucero[1], J.Y. Mutus[1], O. Naaman[1], C. Neill[1], C. Quintana[1], P. Roushan[1], D Sank[1], A. Vainsencher[1], J. Wenner[3], T.C. White[1], S. Boixo[2], R. Babbush[2], V. N. Smelyanskiy[2], H. Neven[2], John M. Martinis[1]

1. Google, Santa Barbara, California 93117
2. Google, Los Angeles, California 90291
3. University of California, Santa Barbara, California 93117

Abstract

Superconducting qubits are an attractive platform for quantum computing since they have demonstrated high-fidelity quantum gates and extensibility to modest system sizes. Nonetheless, an outstanding challenge is stabilizing their energy-relaxation times, which can fluctuate unpredictably in frequency and time. Here, we use qubits as spectral and temporal probes of individual two-level-system defects to provide direct evidence that they are responsible for the largest fluctuations. This research lays the foundation for stabilizing qubit performance through calibration, design and fabrication.

Text (revisions in red)

Superconducting circuits are attractive candidates for implementing qubits as high-fidelity quantum gates have already demonstrated in modest system sizes [1-10]. A primary challenge in scaling such circuits into a quantum computer that can solve practical problems is not only a matter of improving their performance but also stabilizing it. In particular, it has been observed in numerous architectures that qubit energy-relaxation times (T_1) can fluctuate unpredictably by up to an order of magnitude in time [11-16] and in frequency [8,14,16-21]. Since T_1 directly limits gate fidelity, these fluctuations present an obstacle for future scalability.

In past reports, T_1 fluctuations were attributed to quasiparticles [8] or two-level-system (TLS) defects [11-21]. With few exceptions, these conclusions were drawn by analyzing spectrally *or* temporally resolved qubit T_1 data, which offer limited insight into the mechanisms driving relaxation. Here we simultaneously spectrally *and* temporally resolve qubit T_1 to provide direct evidence that the most significant fluctuations can be explained by TLS defects and time-dependent variations in their transition frequencies - a phenomenon known as spectral diffusion. We tentatively explain the spectral diffusion dynamics via the interacting defect model, which is consistent with our observations [14,16,19,22-25]. Interestingly, the T_1 distributions that we extract from spectral and temporal slices of our data are consistent with those observed in other qubit and resonator architectures [7,8,11,12,14,15,26], suggesting that similar defect physics may be at play.

Two-level-system defects have been investigated for decades and were originally used to explain the low-temperature properties of amorphous solids [27]. More recently, they have been identified as a primary source of dielectric loss in superconducting circuits [28]. The microscopic nature of TLS defects is not well understood [29], but they are believed to reside in the amorphous dielectrics present at the material interfaces of superconducting circuits and within Josephson-junctions. Defects can resonantly interact with qubits and serve as a strong energy-relaxation channel [17] (see Fig. 1).

In this report, we spectrally and temporally resolve T_1 of frequency-tunable Xmon transmon qubits [1-3,17,30]. The spectral data is used to identify defects and the temporal data is used to infer their dynamics. The experimental pulse sequence that we use to measure T_1 at a single frequency is as follows: We initialize the qubit into its $|0\rangle$ state, excite it into $|1\rangle$, tune it to the frequency of interest, wait a variable delay time, and then measure its state. To resolve a single T1 curve, we repeat this sequence 2000 times at each of 40 log-spaced delays from 0.01 to 100 μs. Our active initialization protocol takes 7 μs and has fidelity >0.99. Our readout protocol takes 1 μs and has fidelity >0.95. With these protocols, we can quickly resolve a T_1 curve at a single frequency in ~2 seconds, and a spectroscopic T_1 trace across 400 MHz with a 1 MHz resolution in ~15 minutes. We have verified that our qubit-frequency calibration is stable to within ∓ 1 MHz across all of our measurements [30].

A spectrally- and temporally-resolved T_1 dataset for a single qubit is shown in Fig 2a [30]. To better illustrate the dramatic fluctuations in T_1, we show linecuts at constant frequency (Fig. 2b) and constant time (Fig. 2c). We see that T_1 can vary by up to an order of magnitude, and fluctuations between extrema can happen abruptly on 15-minute timescales, and across 5-MHz frequencies. The T_1 distributions of these line cuts are presented in Figs. 2d and e. In time, the distribution can have a single- or multi-modal shape, with the latter being characteristic of telegraphic noise. In frequency, the distributions are weighted heavily near their maxima, but have long tails towards low T_1 due to deep but sparse relaxation resonances (Fig. 2d).

Most regions of strong $1/T_1$ relaxation are characteristic of resonant relaxation into a coupled system, such as a TLS defect [17] or an electromagnetic cavity [30-32]. Importantly, resonant relaxation is not expected for alternative mechanisms such as quasiparticles, capacitor loss, inductor loss, or radiation into a continuum [31,32]. We fit each relaxation resonance to a Lorentzian parametrized by the coupled system's relaxation and transverse coupling rates. We ascribe most resonances to defects since their respective coupling rates range from 50 - 500 kHz, which are consistent with 1 *e*Å dipole moments coupling to electric fields in the qubit capacitor or near it's Josephson junction [17,30]. Furthermore, their measured decoherence rates range from ~0.5 - 20 MHz, which are consistent with defects previously observed similar architectures [17,18, 25]. We ascribe several weak periodic resonances to modes in our qubit control lines and a sharp resonance near 5.6 GHz to bleedthrough of our microwave carrier [30].

We do not analyze the small background fluctuations but believe they can be explained by weakly coupled defects [17], quasiparticles [8], and measurement uncertainty.

To investigate spectral diffusion, we extract the center frequency of each defect's Lorentzian as a function of time, and ascribe it to that defect's transition frequency. We consolidate the transition frequencies of 13 defects across several nominally identical qubits on the same chip (Fig. 3a) and find that their standard deviation evolves in time roughly diffusively as $\sigma(t) = 2Dt^{1/2}$, with the diffusivity $D = 2.5 \mp 0.1$ MHz (hour)$^{-½}$. Nonetheless, a diffusion model by itself oversimplifies the dynamics. Interestingly, defects exhibit a combination of two distinct spectral diffusion regimes - telegraphic and diffusive. Defects in the telegraphic regime experience discrete jumps in frequency, while those in the diffusive regime experience continuous drifts (Fig. 3b). Below we investigate these dynamics.

We do not expect the TLS defects that we observe to exhibit any thermal dynamics in isolation. With transition frequencies of $E_{TLS}/h \sim 5.5$ GHz and a nominal temperature of $T = 15$ mK, their Boltzmann factors are a negligible $\exp(-E_{TLS}/k_B T) \sim 10^{-8}$. Furthermore, strain fluctuations and related defect dynamics [19, 20] should be negligible since our sample temperature is stable to within 2 mK, since the thermal expansion coefficients of all relevant materials are small at cryogenic temperatures, and since strain-defect coupling is generally weak [24]. To explain the spectral diffusion that we observe, we invoke the interacting defect model [14,16,19,22-25], in which TLS defects with $E_{TLS} >> k_B T$ - such as those observed in our T_1 data - interact with thermally fluctuating defects (TF) with $E_{TF} \lesssim k_B T$. Below we introduce this model and describe how telegraphic and diffusive dynamics can emerge from it.

Each TLS and TF defect can be modeled with a tunneling Hamiltonian of the form $\hat{H} = \epsilon\hat{\tau}_z + \Delta\hat{\tau}_x = E\hat{\sigma}_z$ [27]. Here ϵ is the energy asymmetry of the defect's potential energy wells, Δ is the tunneling energy between them, $E = \sqrt{\epsilon^2 + \Delta^2}$ is the transition energy between energy eigenstates, and $\hat{\tau}_i, \hat{\sigma}_i$ are the Pauli matrices in the un-diagonalized and diagonalized bases, respectively. TLS and TF defects couple to each other through the interaction Hamiltonian $\hat{H}_{int} = \frac{1}{2}\Sigma_{ij}^{x,y,z} g_{ij}\hat{\tau}_{z,TLS}\hat{\tau}_{z,TF}$, where the coupling tensor g_{ij} contains dipolar and elastic contributions that depend on the defects' structures, separation, and host material. By virtue of their drastically different energies, TLS and TF defects couple in the off-resonant limit, in which transversal coupling is negligible. The only substantial coupling term is thus $\hat{H}_{zz} = \frac{1}{2} g_{zz}\hat{\tau}_{z,TLS}\hat{\tau}_{z,TF} = \frac{1}{2} g_{\parallel}\hat{\sigma}_{z,TLS}\hat{\sigma}_{z,TF}$, where $g_{\parallel} = g_{zz}(\frac{\epsilon_{TLS}}{E_{TLS}}\frac{\epsilon_{TF}}{E_{TF}})$ [19,25].

To understand how spectral diffusion can emerge from this model, we inspect the energy-level structure of a coupled TLS-TF system (Fig. 3c). In this system, the single-excitation TF and TLS transition frequencies are $E_{TLS}/h = (E_{0,TLS} + g_{\parallel}\langle\hat{\sigma}_{z,TF}\rangle)/h$, and $E_{TF}/h = (E_{0,TF} + g_{\parallel}\langle\hat{\sigma}_{z,TLS}\rangle)/h$, respectively, where E_0/h denotes the uncoupled frequency. From these expressions, we see that the TLS transition frequency depends on the state of its coupled TF, and vice-versa. Therefore, as the TF thermally transitions between its energy eigenstates, the TLS transition

frequency jumps by $2g_{||}/h$, which is observed as telegraphic spectral diffusion. The rate of telegraphic jumping is determined by the TF's phononic excitation and relaxation rates, which are $\Gamma_{e\to g} = \alpha\, \Delta_{TF}{}^2 E_{TF} \coth(E_{TF}/2k_B T)$ and $\Gamma_{g\to e} = \exp(-E_{TF}/k_B T)\Gamma_{e\to g}$, respectively. Here α is a constant related to the phonon-TF coupling rate, material density, and the speed of sound [23-25, 27]. Diffusive spectral diffusion is expected to emerge in the bath limit of this model, in which a single TLS is coupled to many TFs with distinct coupling and telegraphic jumping rates [16].

We now analyze our observations in the context of the interacting defect model and confirm that they are consistent [30]. The largest telegraphic jump that we observe is ~ 60 MHz, which corresponds to a TLS-TF coupling rate $g_{||}/h$ = 30 MHz. This coupling magnitude makes physical sense since it corresponds to the interaction of two collinear 1 *e*Å dipoles separated by ~35 nm in a material with a relative permittivity of 10. The average telegraphic jump rates $\Gamma = (\Gamma_{g\to e} + \Gamma_{e\to g})/2$ that we observe range from ~ 50 uHz to 5 mHz, and they are roughly distributed as $\sim\Gamma^{-1}$. This distribution is expected for tunneling defects [24], but the range is somewhat surprising, since typical TLS relaxation rates are ~1 MHz [25]. This disparity may be explained by the quadratic scaling of $\Gamma_{e\to g}$ on the tunneling energy Δ, which can vary from uHz to GHz for defects in similar materials [16, 19, 25]. The scaling of $\Gamma_{e\to g}$ on the transition energy E cannot close this disparity. For several defects where many telegraphic jumps are observed, we estimate the TF energy $E_{TF}/k_B T = \ln(\Gamma_{e\to g}/\Gamma_{g\to e})$, which ranges from 0.18 to 0.99. This is consistent with our primary hypothesis that spectral diffusion is driven by thermal fluctuators.

To estimate the density of TF defects and to understand the relationship between the telegraphic and diffusive regimes, we run a Markov-Chain Monte Carlo simulation of interacting defect dynamics in a thin film representative of the interfacial dielectrics in our qubit circuit. Since the diffusivity of TLS transitions is expected to depend strongly on TF density, we use it to connect simulation to experiment. We find that our experimentally measured diffusivity $D = 2.5 \mp 0.1$ MHz $(\text{hour})^{-½}$ is consistently reproduced by our simulation at TF densities above 10^4 GHz^{-1} μm^{-3} (~25×10^{20} eV^{-1} cm^{-3}). Furthermore, at a fixed density of ~10^4 GHz^{-1} μm^{-3}, the simulation qualitatively reproduces virtually all of our diffusive and telegraphic data (see Fig. S3 in ref. 30). This density is ~10x higher than the densities typically quoted for bulk dielectrics, but this is not unexpected for interfacial thin films [22]. These simulations demonstrate that the observed spectral diffusion dynamics can emerge from the interacting defect model at a single TF density that is physically plausible.

We spectrally and temporally resolved qubit T_1. In these data we identified single TLS defects and tracked their spectral diffusion dynamics, which we attribute to the interacting defect model. We find that defects and their spectral diffusion are directly responsible for the most significant time- and frequency-domain qubit T_1 fluctuations. Interestingly, the T_1 distributions that we

extract from time- and frequency-domain cuts of our data are qualitatively similar to those seen in in planar resonators [11,12,26], fixed-frequency 3D transmon qubits [14], fixed-frequency planar transmon qubits [7,15], and flux qubits [8]. This correspondence suggests that TLS defects may be the source of T_1 fluctuations in many superconducting quantum computing architectures.

Our results suggest that understanding defect properties at scale is important for stabilizing and improving the energy-relaxation times of superconducting circuits. In the short term, defect data should guide qubit calibration protocols. For example, defects' diffusivity and coherence properties should inform the algorithms that are used to select tunable qubits' frequencies and how often those algorithms are run. In the long term, defect data should guide qubit design and fabrication parameters. For example, the relationship between spectral diffusion and defect density suggests that correlation studies can be used to identify defective circuit components and materials. Ultimately, improved qubit calibration, circuit design, and fabrication will likely be necessary to manufacture and operate a quantum computer that can solve practical problems.

Acknowledgements

This work was supported by Google. C.Q. and Z.C. acknowledge support from the National Science Foundation Graduate Research Fellowship under Grant No. DGE-1144085. Devices were made at the UC Santa Barbara Nanofabrication Facility, a part of the NSF funded National Nanotechnology Infrastructure Network.

References

1. R. Barends, J. Kelly, A. Megrant, A. Veitia, D. Sank, E. Jeffrey, T. C. White, J. Mutus, A. G. Fowler, B. Campbell, Y. Chen, Z. Chen, B. Chiaro, A. Dunsworth, C. Neill, P. O'Malley, P. Roushan, A. Vainsencher, J. Wenner, A. N. Korotkov, A. N. Cleland, J. M. Martinis, Nature 508, 500-503 (2014).
2. J. Kelly, R. Barends, A. G. Fowler, A. Megrant, E. Jeffrey, T. C. White, D. Sank, J. Y. Mutus, B. Campbell, Yu Chen, Z. Chen, B. Chiaro, A. Dunsworth, I.-C. Hoi, C. Neill, P. J. J. O'Malley, C. Quintana, P. Roushan, A. Vainsencher, J. Wenner, A. N. Cleland, J. M. Martinis, Nature 519, 66-69 (2015).
3. R. Barends, A. Shabani, L. Lamata, J. Kelly, A. Mezzacapo, U. Las Heras, R. Babbush, A. G. Fowler, B. Campbell, Yu Chen, Z. Chen, B. Chiaro, A. Dunsworth, E. Jeffrey, E. Lucero, A. Megrant, J. Y. Mutus, M. Neeley, C. Neill, P. J. J. O'Malley, C. Quintana, P. Roushan, D. Sank, A. Vainsencher, J. Wenner, T. C. White, E. Solano, H. Neven, J. M. Martinis, Nature 534, 222-226 (2016).
4. Nissim Ofek, Andrei Petrenko, Reinier Heeres, Philip Reinhold, Zaki Leghtas, Brian Vlastakis, Yehan Liu, Luigi Frunzio, S. M. Girvin, L. Jiang, Mazyar Mirrahimi, M. H. Devoret, R. J. Schoelkopf, Nature 536, 441 (2016).
5. M.A. Rol, C.C. Bultink, T.E. O'Brien, S.R. de Jong, L.S. Theis, X.Fu, F.Luthi, R.F.L. Vermeulen, J.C. de Sterke, A. Bruno, D. Deurloo, R.N. Schouten, F.K. Wilhelm, L. DiCarlo, Phys. Rev. Appl. 7, 041001 (2017).

6. J. S. Otterbach, R. Manenti, N. Alidoust, A. Bestwick, M. Block, B. Bloom, S. Caldwell, N. Didier, E. Schuyler Fried, S. Hong, P. Karalekas, C. B. Osborn, A. Papageorge, E. C. Peterson, G. Prawiratmodjo, N. Rubin, Colm A. Ryan, D. Scarabelli, M. Scheer, E. A. Sete, P. Sivarajah, Robert S. Smith, A. Staley, N. Tezak, W. J. Zeng, A. Hudson, Blake R. Johnson, M. Reagor, M. P. da Silva, C. Rigetti, arxiv: 1712.05771 (2017).
7. IBM Q Experience, *https://quantumexperience.ng.bluemix.net/qx/devices*
8. F. Yan, S. Gustavsson, A. Kamal, J. Birenbaum, A. P. Sears, D. Hover, T. J. Gudmundsen, D. Rosenberg, G. Samach, S. Weber, J. L. Yoder, T. P. Orlando, J. Clarke, A. J. Kerman, W. D. Oliver, Nat. Commun. 7, 12964 doi:10.1038/ncomms12964 (2016).
9. G. Wendin, Rep. Prog. Phys. 80, 106001 (2017).
10. X. Gu, A. F. Kockum, A. Miranowicz, Y. Liu, F. Nori, Phys. Rep. 718-719, 1-102 (2017).
11. A. Megrant, C. Neill, R. Barends, B. Chiaro, Y. Chen, L. Feigl, J. Kelly, E. Lucero, M. Mariantoni, P. J. J. O'Malley, D. Sank, A. Vainsencher, J. Wenner, T. C. White, Y. Yin, J. Zhao, C. J. Palmstrøm, J. M. Martinis, Appl. Phys. Lett. 100, 113510 (2012).
12. C. Neill, A. Megrant, R. Barends, Y. Chen, B. Chiaro, J. Kelly, J. Y. Mutus, P. J. J. O'Malley, D. Sank, J. Wenner, T. C. White, Y. Yin, A. N. Cleland, J. M. Martinis, Appl. Phys. Lett. 103, 072601 (2013).
13. P. Macha, S. H. W. van der Ploeg, G. Oelsner, E. Il'ichev, H.-G. Meyer, S. Wunsch, M. Siegel, Appl. Phys. Lett. 96, 062503 (2010).
14. C. Müller, J. Lisenfeld, A. Shnirman, S. Poletto, Phys. Rev. B 92, 035442 (2015).
15. J. B. Chang, M. R. Vissers, A. D. Corcoles, M. Sandberg, J. Gao, D. W. Abraham, J. M. Chow, J. M. Gambetta, M. B. Rothwell, G. A. Keefe, M. Steffen, D. P. Pappas, Appl. Phys. Lett. 103, 012602 (2013).
16. S. Meißner, A. Seiler, J. Lisenfeld, A. V. Ustinov, G. Weiss, arXiv:1710.05883 (2017).
17. R. Barends, J. Kelly, A. Megrant, D. Sank, E. Jeffrey, Y. Chen, Y. Yin, B. Chiaro, J. Mutus, C. Neill, P. O'Malley, P. Roushan, J. Wenner, T. C. White, A. N. Cleland, J. M. Martinis, Phys. Rev. Lett. 111, 080502 (2013).
18. Y. Shalibo, Y. Rofe, D. Shwa, F. Zeides, M. Neeley, J. M. Martinis, N. Katz, Phys. Rev. Lett. 105, 177001 (2010).
19. J. Lisenfeld, G. J. Grabovskij, C. Muller, J. H. Cole, G. Weiss, A. V. Ustinov, Nat. Commun. 10.1038/ncomms7182 (2014)
20. G. J. Grabovskij, T. Peichl, J. Lisenfeld, G. Weiss, A. V. Ustinov, Science 338, 232 (2012).
21. M. Stern, G. Catelani, Y. Kubo, C. Grezes, A. Bienfait, D. Vion, D. Esteve, P. Bertet, Phys. Rev. Lett., 113, 123601 (2014)
22. L. Faoro, L. B. Ioffe, Phys. Rev. Lett. 109, 157005 (2012).
23. J. Burnett, L. Faoro, I. Wisby, V. L. Gurtovoi, A. V. Chernykh, G. M. Mikhailov, V. A. Tulin, R. Shaikhaidarov, V. Antonov, P. J. Messon, A. Y. Tzalenchuk, T. Lindstrom, Nat. Commun. 10.1038/ncomms5119 (2013).
24. L. Faoro, L. B. Ioffe, Phys. Rev. B 91, 014201 (2015).
25. J. Lisenfeld, A. Bilmes, S. Matityahu, S. Zanker, M. Marthaler, M. Schechter, G. Schon, A. Shnirman, G. Weiss, A. Ustinov, Sci. Reports 6, 23786 (2016).

26. K. Geerlings, S. Shankar, E. Edwards, L. Frunzio, R. J. Schoelkopf, Appl. Phys. Lett. 100, 192601 (2012).
27. W. A. Phillips, J. Low Temp. Phys. 7, 351–360 (1972).
28. J. M. Martinis, K. B. Cooper, R. McDermott, M. Steffen, M. Ansmann, K. D. Osborn, K. Cicak, S. Oh, D. P. Pappas, R. W. Simmonds, C. C. Yu, Phys. Rev. Lett. 95, 210503 (2005).
29. C. Muller, J. H. Cole, J. Lisenfeld, arXiv: 1705.01108 (2017).
30. See Supplementary Materials at ___ for additional data, analysis, and discussion.
31. A. A. Houck, J. A. Schreier, B. R. Johnson, J. M. Chow, J. Koch, J. M. Gambetta, D. I. Schuster, L. Frunzio, M. H. Devoret, S. M. Girvin, R. J. Schoelkopf, Phys. Rev. Lett. 101, 080502 (2008).
32. J. Koch, T. M. Yu, J. M. Gambetta, A. A. Houck, D. I. Schuster, J. Majer, A. Blais, M. H. Devoret, S. M. Girvin, and R. J. Schoelkopf, Phys. Rev. A 76, 042319 (2007).

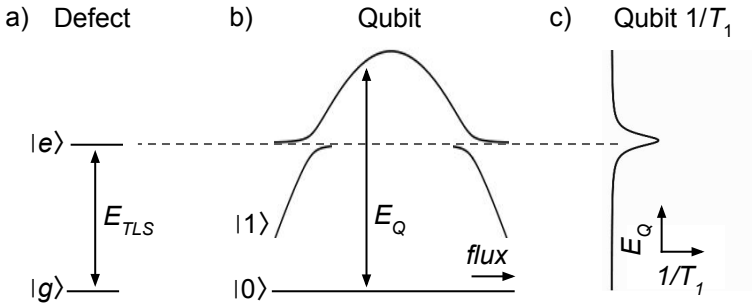
a) Defect
b) Qubit
c) Qubit $1/T_1$
$|e\rangle$
$|g\rangle$
E_{TLS}
$|1\rangle$
$|0\rangle$
E_Q
flux
E_Q
$1/T_1$

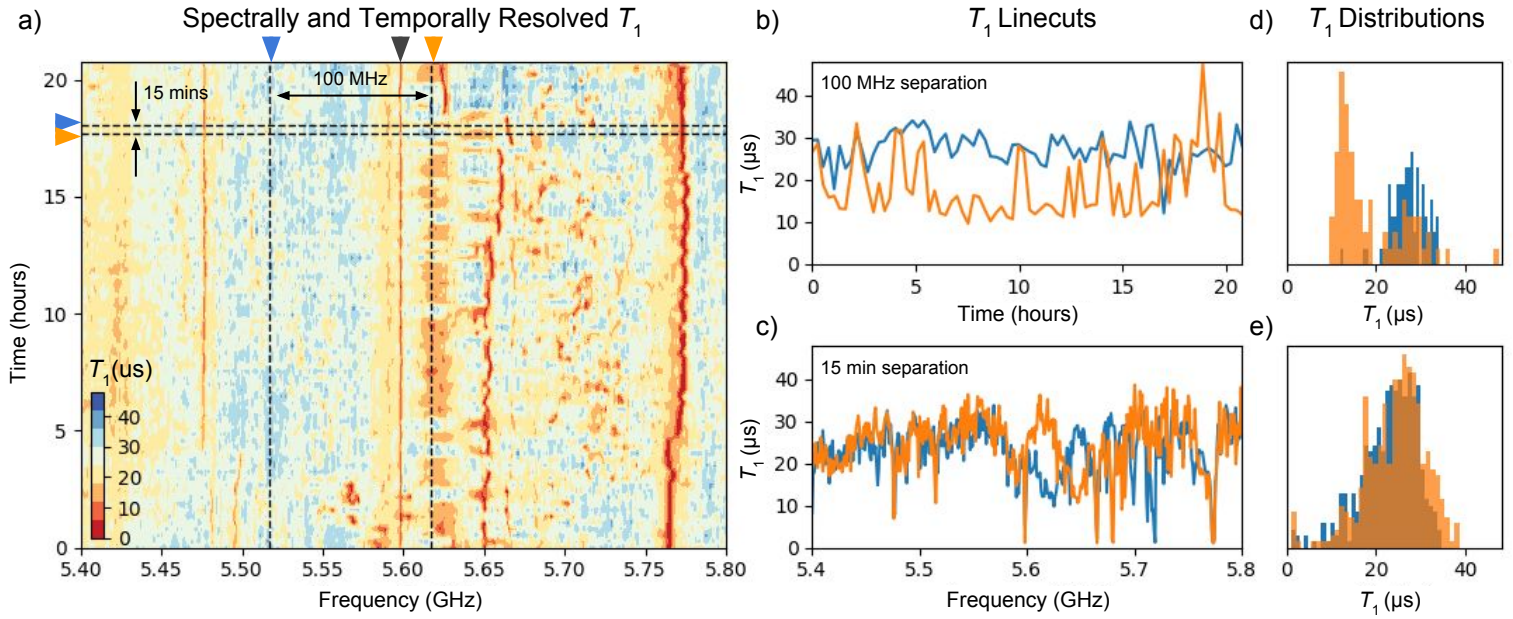
a)
Spectrally and Temporally Resolved T_1
15 mins
100 MHz
T_1(us)
40
30
20
10
0
Time (hours)
Frequency (GHz)
b)
T_1 Linecuts
100 MHz separation
T_1 (μs)
Time (hours)
c)
15 min separation
T_1 (μs)
Frequency (GHz)
d)
T_1 Distributions
T_1 (μs)
e)
T_1 (μs)

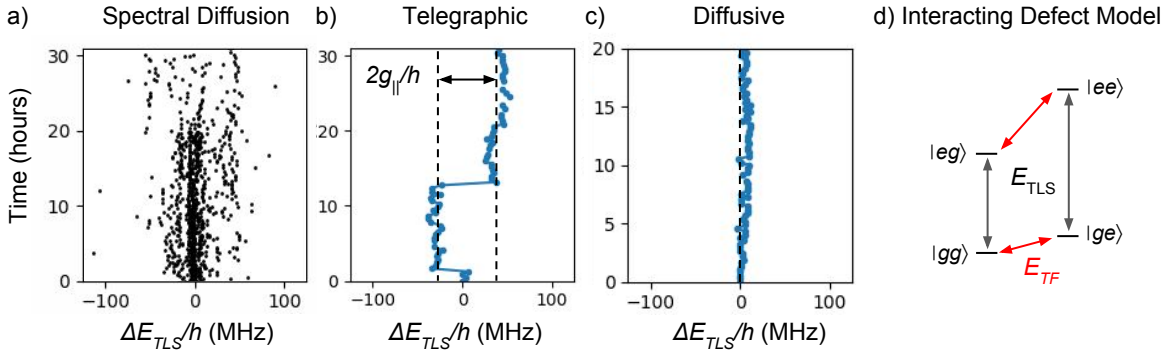
a)
Spectral Diffusion
b)
Telegraphic
c)
Diffusive
d) Interacting Defect Model
Time (hours)
$\Delta E_{TLS}/h$ (MHz)
$2g_{\parallel}/h$
$|ee\rangle$
$|eg\rangle$
$|ge\rangle$
$|gg\rangle$
E_{TLS}
E_{TF}